the various combinations of experimental conditions that may be encountered.

The foregoing analysis has uncovered diffraction-theoretical reasons to account for the observations of large relative changes of Borrmann–Lehmann fringe spacings produced by strain gradients too small to affect *Pendellösung* spacings noticeably in a conventional topograph. In all but the most perfect crystals, $Z_a/2P_E$ is unlikely to be small compared with unity. For example, if f arose from a uniform dilatation gradient normal to the Bragg planes, then a gradient as low as $10^{-6}\,\text{mm}^{-1}$ would make $Z_a \simeq 0\cdot1$ when diffraction parameters similar to those operating in the experiments illustrated in § 4 applied. Then with small values of P_E, about $0\cdot1$ say, changes in fringe spacing of order 100% would be produced. This analysis justifies the suggestion previously made (Lang *et al.*, 1986) that experiments of the Borrmann–Lehmann interference type deserve serious consideration for development and application in crystal assessment work. The origin of the high sensitivity may be qualitatively pictured by an analogy with X-ray interferometry. It can be said that the action of combining rays OW and OQW, which take quite different paths through the distorted crystal, turns the specimen into its own interferometer.

References

BONSE, U. (1964). *Z. Phys.* **177**, 385–423.
BORRMANN, G. & LEHMANN, K. (1963). *Crystallography and Crystal Perfection*, edited by G. N. RAMACHANDRAN, pp. 101–108. London, New York: Academic Press.
DAWSON, B. (1967). *Proc. R. Soc. London Ser. A*, **298**, 264–288.
HART, M. & LANG, A. R. (1965). *Acta Cryst.* **19**, 73–77.
HATTORI, H., KURIYAMA, H. & KATO, N. (1965). *J. Phys. Soc. Jpn*, **20**, 1047–1050.
KAMBE, K. (1965). *Z. Naturforsch. Teil A*, **20**, 770–786.
KAMBE, K. (1968). *Z. Naturforsch. Teil A*, **23**, 25–43.
KATO, N. (1961a). *Acta Cryst.* **14**, 526–532.
KATO, N. (1961b). *Acta Cryst.* **14**, 627–636.
KATO, N. (1963). *J. Phys. Soc. Jpn*, **18**, 1785–1791.
KATO, N. (1964a). *J. Phys. Soc. Jpn*, **19**, 67–77.
KATO, N. (1964b). *J. Phys. Soc. Jpn*, **19**, 971–985.
KATO, N. (1968). *J. Appl. Phys.* **39**, 2231–2237.
KATO, N. (1974). In *X-ray Diffraction*, by L. V. AZÁROFF, R. KAPLOW, N. KATO, R. J. WEISS, A. J. C. WILSON & R. A. YOUNG, Chs. 4, 5. New York: McGraw-Hill.
KATO, N. & ANDO, Y. (1966). *J. Phys. Soc. Jpn*, **21**, 964–968.
KOWALSKI, G. & LANG, A. R. (1986). *J. Appl. Cryst.* **19**, 224–228.
KOWALSKI, G. & LANG, A. R. (1987). *Acta Cryst.* A**43**, C220.
LANG, A. R. (1957). *Acta Metall.* **5**, 358–364.
LANG, A. R. (1983). *Rev. Sci. Instrum.* **54**, 897–899.
LANG, A. R., KOWALSKI, G., MAKEPEACE, A. P. W. & MOORE, M. (1986). *Acta Cryst.* A**42**, 501–510.
LEHMANN, K. & BORRMANN, G. (1967). *Z. Kristallogr.* **125**, 234–248.
MAI, Z.-H. & ZHAO, H. (1989). *Acta Cryst.* A**45**, 602–609.
PENNING, P. & POLDER, P. (1961). *Philips Res. Rep.* **16**, 419–440.
SAKA, T., KATAGAWA, T. & KATO, N. (1972a). *Acta Cryst.* A**28**, 102–113.
SAKA, T., KATAGAWA, T. & KATO, N. (1972b). *Acta Cryst.* A**28**, 113–120.
TAKAGI, S. (1962). *Acta Cryst.* **15**, 1131–1132.
TAKAGI, S. (1969). *J. Phys. Soc. Jpn*, **26**, 1239–1253.
TAUPIN, D. (1964). *Bull. Soc. Fr. Minéral. Cristallogr.* **87**, 469–511.

Direct Calculation of Unambiguous Electron-Density Distributions of Langmuir–Blodgett Films Normal to the Membrane Plane

By MATTHIAS VON FRIELING AND HANS BRADACZEK

Institut für Kristallographie, Freie Universität Berlin, Takustrasse 6, D-1000 Berlin 33, Federal Republic of Germany

Abstract

In regard to X-ray diffraction, Langmuir–Blodgett (LB) films consisting of lipid bilayers represent a 'one-dimensional crystal' with a very small number of unit cells in the direction of stacking. Such bounded systems yield X-ray diffraction diagrams which, in certain respects, contain more information than those of the conventional effectively infinite single crystals. This additional information consists of the profiles of the broadened reflections and their dislocation from the reciprocal-lattice points. These profiles are specific for each different structure and hence enable the direct calculation of unambiguous electron-density distributions from a single set of intensity data. At first, the Q function (the generalized Patterson function), *i.e.* the distance statistics of the structure sought after is calculated from the intensity data.

Thereafter, the unambiguous convolution square root of the Q function must be determined, which is identical to the unknown electron-density distribution. For this purpose two mathematically completely different methods were established and compared. They were applied to diffraction patterns of Langmuir–Blodgett films of simple synthetic lipids with characteristic molecular subunits and showed identical results within the experimental resolution. This verifies the structures and the methods to calculate them. Furthermore, all features of the simple structures were compatible with the expectations. All one-dimensional electron-density distributions showed the common features of lipid bilayers. The characteristic molecular subunits can be recognized and reveal some interesting details. In general, they yield information about orientation, conformation and localization of molecular subunits and membrane components.

1. Introduction

The well known phase problem of crystallography has greatly hindered the structure determination of natural and artificial bilayer stacks (*e.g.* LB films) by X-ray diffraction. Different methods have been used to determine the signs of the lamellar reflections but all of them remain somewhat unsatisfactory:

(*a*) The trial-and-error method to calculate intensities from electron-density models and to compare them with measured intensities (Worthington, 1969) yields rather inexact results and one must know a good deal about the structure in advance.

(*b*) The pattern-recognition approach of Luzatti, Tardieu & Taupin (1972) is just a systematized approach using the same method.

(*c*) The heavy-atom method (Akers & Parsons, 1970) is not applicable in all cases and biological membranes, in particular, can undergo structural changes with the introduction of heavy atoms.

(*d*) The same uncertainty impairs the swelling technique (Worthington, King & McIntosh, 1973; Franks & Levine, 1981) which is, nevertheless, most widely used so far. By inserting water layers between the head-group layers an attempt is made to separate the overlapping Q_0 functions (Worthington, King & McIntosh, 1973; Franks & Levine, 1981; Hosemann & Bagchi, 1962) and to sample the continuous Fourier transform F_0 of a single unit cell by measuring different states of swelling (Franks & Levine, 1981). At each zero point of F_0 its sign changes and hence the signs of the reflections can be recognized.

The bilayer structure itself must not be changed during the swelling process. Many measurements are necessary for the determination of one set of signs. Although the methods mentioned above have been applied successfully in certain cases (Akers & Parsons, 1970; Franks & Lieb, 1979; Worthington, 1973*a*, *b*; Tardieu, Luzatti & Reman, 1973; Franks,

Arunachalam & Caspi, 1978) a quicker reliable method for the routine application was needed to determine the structures of a larger number of Langmuir–Blodgett films.

2. Theory

A bounded structure can be described after Ewald (1940) in the following way:

$$\rho(x) = \rho_0(x) \frown [z(x)s(x)] \qquad (1)$$

$x =$ coordinate of the one-dimensional physical space; $\frown =$ symbol for convolution; $\rho(x) =$ electron-density distribution; $\rho_0(x) =$ electron-density distribution of a single unit cell; $z(x) =$ lattice peak function; $s(x) =$ bounded shape function.

This equation means that an infinite lattice peak function $z(x)$ is multiplied with a bounded shape function $s(x)$ resulting in a lattice peak function which is now bounded too. Subsequently, the bounded lattice peak function is convoluted with the electron-density distribution ρ_0 of a single unit cell which is equivalent to putting together the unaltered unit cells. In this way a bounded structure is created which is periodic within its limits.
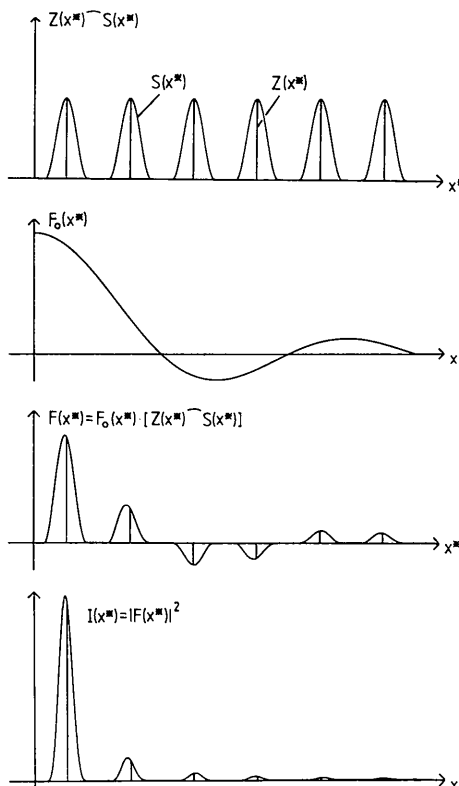

Fig. 1. Emergence of broadened reflections with structure-specific profiles [the side maxima of the $(\sin x)/x$ type functions have been omitted; the calibrations of the ordinate axes are arbitrary].

The Fourier transform of (1) is given by

$$F(x^*) = F_0(x^*)[Z(x^*)\frown S(x^*)]. \qquad (2)$$

$x^* =$ coordinate of the one-dimensional reciprocal space; $F(x^*) =$ Fourier transform of the structure $\rho(x)$; $F_0(x^*) =$ Fourier transform of the structure $\rho_0(x)$ of a single unit cell; $Z(x^*) =$ Fourier transform of the lattice peak function $z(x)$; $S(x^*) =$ Fourier transform of the shape function $s(x)$. $Z(x^*)$ is a lattice peak function again. $S(x^*)$ is a function of the type $(\sin x/x)$. The smaller $s(x)$, the broader $S(x^*)$ and vice versa, i.e. systems with only a few unit cells and a small shape function such as LB films will give broadened reflections compared to the reflections of effectively infinite single crystals (cf. Fig. 1). This can be proved experimentally (Lesslauer & Blasie, 1972; Lesslauer, 1974b; von Frieling, 1989) and is the reason for the unambiguous relationship between the structure and the X-ray diffraction diagram because the $S(x^*)$ at each reciprocal-lattice point is multiplied with $F_0(x^*)$. Therefore, each function $S(x^*)$ has a characteristic profile and its centre of gravity is dislocated slightly from the reciprocal-lattice points (cf. Fig. 1). The same is true for the X-ray reflections. $F_0(x^*)$, of course, is different for each structure and therefore the profiles of the reflections and their dislocations are structure specific. The continuous intensity distribution of a bounded system is different for each structure. Fig. 1 shows the emergence of broadened reflections $[I(x^*)]$ with a structure-specific profile.

In larger systems (single crystals), where the shape functions are effectively infinite in atomic dimensions, the reflections become very sharp and their profiles are not detectable.

By calculating the Fourier transform of the continuous intensity distribution of only a few unit cells one does not obtain the ideally periodic Patterson function but the damped periodic Q function. The Patterson function is the borderline case for infinite structures of the general Q function (Hosemann & Bagchi, 1962). It was proved by Hosemann & Bagchi (1952, 1962) that the Q function of bounded centrosymmetric structures has a unique convolution square root which is the sought-after structure. Consequently, an unambiguous structure analysis of bounded centrosymmetric systems is possible with X-ray diffraction. LB films ideally fulfil this condition.
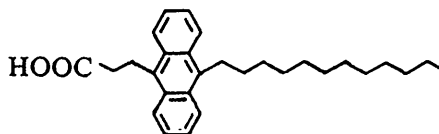
3. Experimental and computational details

3.1. Preparing and measuring the LB films

LB films of 7-(2-anthryl)-1-heptanoic acid (2A7)
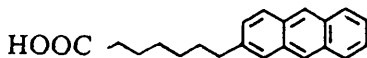
and 3-[9-(10-dodecyl)anthryl]-1-propionic acid (9,10A12)

were formed as described elsewhere on a solution of $CdCl_2$ (Durfee, Storck, Willig & von Frieling, 1987). Films of stearic acid (Sigma) were prepared on hydrophobic glass slides (van der Auweraer & Willig, 1985) using a circular trough after Fromherz (1975). The monolayer was transferred from a subphase solution containing 3×10^{-5} M $BaCl_2$ and 4×10^{-4} M $KHCO_3$ at pH 7 at a constant surface pressure of 30 mN m^{-1} and a transfer speed of 7·5 or 13 mm min^{-1} respectively. The pH was adjusted with HCl. The lipids were dissolved in $CHCl_3$ except for one LB film of barium stearate where petroleum ether was used.

Low-angle X-ray diffraction was performed with a powder diffractometer. Cu $K\alpha$ (nickel filtered) radiation ($\lambda = 1\cdot5418$ Å) was produced with accelerating voltages of 40 kV at 30 mA (2A7 and 9,10A12) and 45 kV at 35 mA (stearic acid). Data were collected with a proportional counter by the θ-2θ method and corrected for Lorentz and polarization effects after the method of Blaurock & Worthington (1966) in a way appropriate for planar multilayered structures:

$$I_c = hI_m[1 + (\cos 2\theta)^2]/2 \qquad (3)$$

where I_c are the corrected intensities, I_m the measured intensities, h the order of reflection and θ the Bragg angle. The scattering of the glass substrate was measured separately and subtracted.

3.2. Direct calculation of electron-density distributions

First, the inverse Fourier transformation of the continuous distribution of corrected intensities is calculated, yielding the Q function:

$$Q(x) = (2/d) \sum_h I_c \cos(2\pi xh/d) \qquad (4)$$

where x is the coordinate normal to the membrane plane and d is the periodicity.

To carry out the deconvolution of Q Hosemann & Bagchi proposed both a recursion method (1962) and a method using convolution polynomials (1952). They are very sensitive to experimental errors, however, and even to rounding errors of the computer. They were rarely applied with success (Kreutz, 1970; Lesslauer, Cain & Blasie, 1971; Lesslauer & Blasie, 1972). For this reason, Pape (1974) and Bradaczek & Luger (1978) independently developed two mathematically completely different procedures to calculate the convolution square root. Pape (1974) uses the Q_0 function, the Q function of a single unit cell, which can be separated from the Q function (Kreutz, 1970;

Hosemann & Baghi, 1953), while Bradaczek & Luger (1978) directly use a period of the Q function. It was shown by von Frieling (1989) that the method of Pape can be applied to the Q function as well with the same result as for Q_0. Both techniques use all values of one period of Q_0 or Q, respectively, for the calculation of each value of the electron-density distribution and hence they are much more accurate than the recursion process of Hosemann & Bagchi (1962).

Pape's procedure is a Fourier-analytical deconvolution method; it neglects the left-hand half of the centrosymmetric Q_0 function and describes the remaining asymmetric right-hand half by a Fourier series which is, of course, not real but has sine coefficients as well as cosine coefficients differing from zero. The sine coefficients are related to the cosine coefficients (with signs) and can be developed into a linear system of equations which yields the signs of the cosine coefficients as its solution (not the complete coefficients) and leads to one unit cell ρ_0 of the structure.

The method of Bradaczek & Luger (1978) consists of the solution of the convolution integral (5) for $\rho(x)$ by successive approximations:

$$Q(x) = \int_{-\infty}^{+\infty} \rho(v)\rho(v-x)\,\mathrm{d}v \qquad (5)$$

$x, v =$ coordinates of the one-dimensional physical space. $Q^{\cdot}$ as well as ρ are expressed as sampled functions, point by point. Equation (5) is then comprehended as a linear system of equations. An arbitrary first approximation of the unknown structure is written as a matrix, inverted and multiplied with Q written as a vector. The result is a second approximation.

Repetition of the procedure with the average of the first and the second approximation, of the second and the third approximation and so on leads to a very quickly converging refinement which is independent of the first approximation (Bradaczek & Luger, 1978). Depending on the attainable resolution determined by the experiment, four to six refinement cycles are absolutely enough. The closer the first approximation is to the unknown structure, the faster is the refinement. We used a straight line as first approximation with two higher values at its ends to simulate the head-group maxima.

In summary, there exist two straightforward procedures for the calculation of the electron-density distribution from only a single set of intensity data of bounded one-dimensional systems. In the following their first application to LB films is shown. Dr Pape kindly gave his deconvolution program to us, and the method of Bradaczek & Luger (1978) was programmed by us. Both programs were run on a VAX (Digital).

4. Results

The measured LB films show seven to 43 sharp lamellar reflections depending on the kind of molecule and on the number of deposited bilayers, indicating their high state of order (Figs. 2-7).
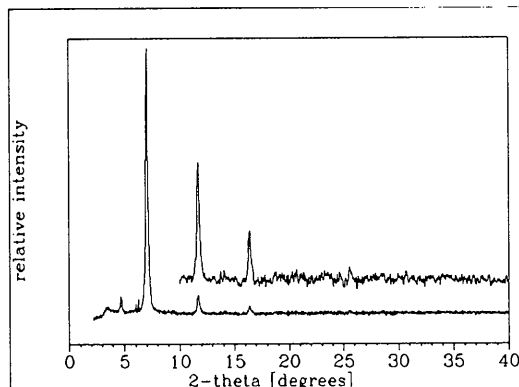

Fig. 2. X-ray diffraction pattern of five bilayers of 2A7 formed at a subphase pH of 4·9 and a transfer pressure of 18 mN m^{-1}. The periodicity is 37·8 Å.
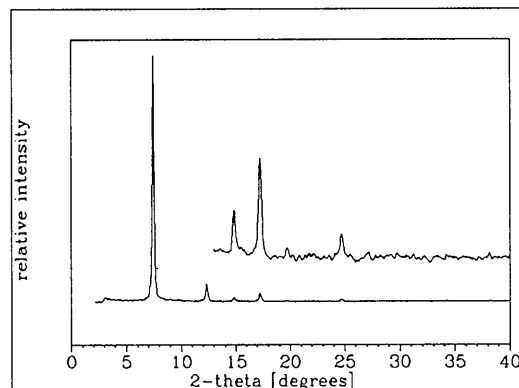

Fig. 3. X-ray diffraction pattern of ten bilayers of 2A7 formed at a subphase pH of 4·9 and a transfer pressure of 21 mN m^{-1}. The periodicity is 36 Å.
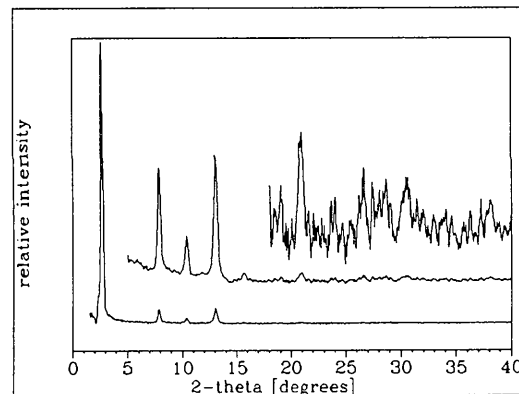

Fig. 4. X-ray diffraction pattern of ten bilayers of 9,10A12 formed at a subphase pH of 4·9 and a transfer pressure of 21 mN m^{-1}. The periodicity is 34 Å.

In Fig. 2 the X-ray diffraction pattern of five bilayers of 2A7 is shown. Lamellar reflections up to the seventh order can be seen (first, fourth and sixth order missing), representing a bilayer periodicity of 37·8 Å. Fig. 3 shows the diffraction pattern of a ten-bilayer stack of 2A7 transferred at a higher surface pressure (highest observed order: tenth; missing: first, second, fourth, eighth and ninth order; $d = 36$ Å). Fig. 4 depicts the diffraction pattern of ten bilayers of 9,10A12 (highest observed order: eighth; missing: second and seventh order; $d = 34$ Å) and Fig. 5 again the reflections of ten bilayers of the same substance
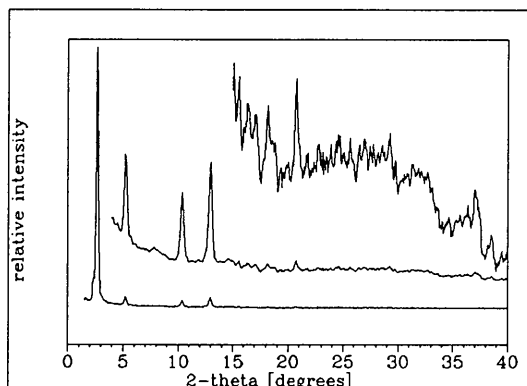
Fig. 5. X-ray diffraction pattern of ten bilayers of 9,10A12 formed at a subphase pH of 6·0 and a transfer pressure of 21 mN m^{-1}. The periodicity is 34·2 Å.
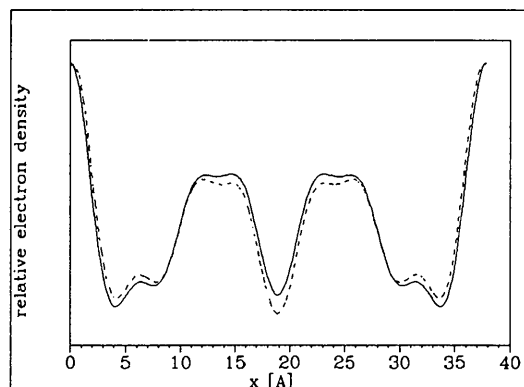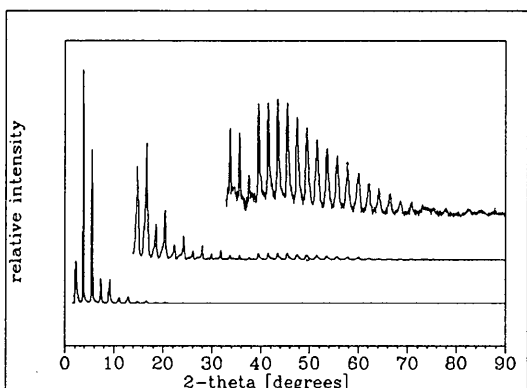
Fig. 6. X-ray diffraction pattern of 85 bilayers of barium stearate formed at a subphase pH of 7·0, a transfer pressure of 30 mN m^{-1} and a transfer speed of 13 mm min^{-1}.

Fig. 7. X-ray diffraction pattern of 50 bilayers of barium stearate formed at a subphase pH of 7·0, a transfer pressure of 30 mN m^{-1} and a transfer speed of 7·5 mm min^{-1}.
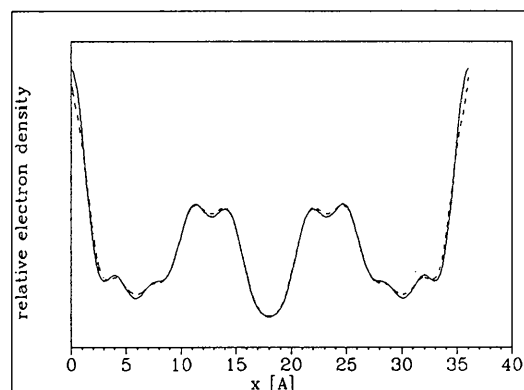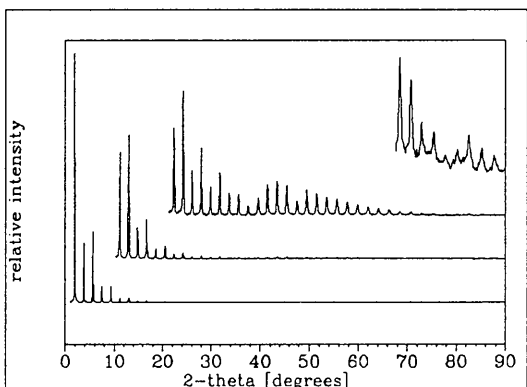
Fig. 8. Electron-density distribution across a bilayer of 2A7 formed at a transfer pressure of 18 mN m^{-1} (resolution 5·4 Å).

Fig. 9. Electron-density distribution across a bilayer of 2A7 formed at a transfer pressure of 21 mN m^{-1} (resolution 3·6 Å).
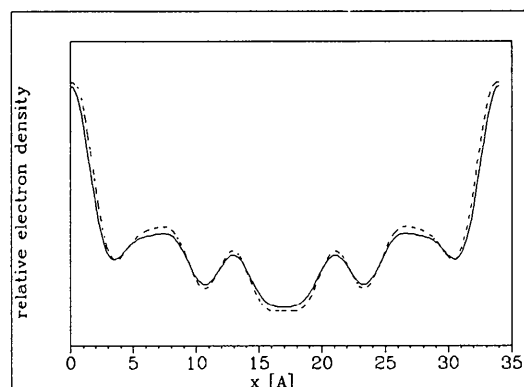
Fig. 10. Electron-density distribution across a bilayer of 9,10A12 formed at pH 4·9 (resolution 4·25 Å).

transferred at a higher pH (highest observed order: eighth; missing: third, sixth and seventh order; $d = 34 \cdot 2$ Å). Figs. 6 and 7 impressively show the capability of the LB method. 85 bilayers of barium stearate give 36 reflections, 50 bilayers of the same substance transferred at a lower transfer speed even give 43 reflec-
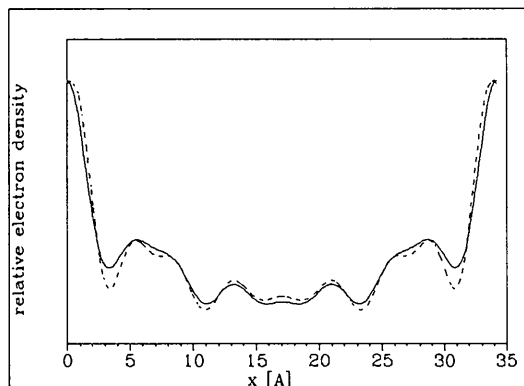

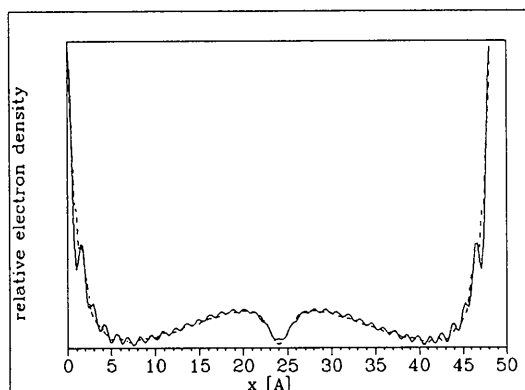Fig. 11. Electron-density distribution across a bilayer of 9,10A12 formed at pH 6·0 (resolution 4·28 Å).

Fig. 12. Electron-density distribution across a bilayer of barium stearate at 1·34 Å resolution. The stearic acid was dissolved in petroleum ether.
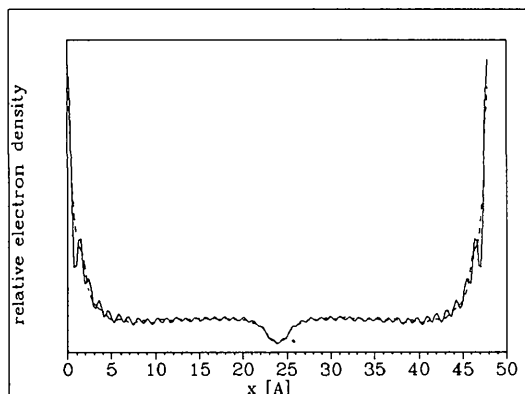

Fig. 13. Electron-density distribution across a bilayer of barium stearate at 1·11 Å resolution. The stearic acid was dissolved in CHCl₃.

tions. Figs. 8–13 show the corresponding relative electron-density distributions normal to the bilayer plane. In each figure the result after the method of Pape (1974) (full curves) is compared to that after Bradaczek & Luger (1978) (dotted curves). The electron-density distributions clearly indicate Y-type films (Blodgett, 1935) in all cases and show the common features of lipid bilayers, i.e. electron-density maxima in the head-group region and minima in the middle. Furthermore, the characteristic molecular subunits (aliphatic chains and anthracene residues) can be recognized and reveal some interesting details. Absolute values of electron density are not obtained because the zeroth-order reflection cannot be measured.

5. Discussion

First of all, the results of the methods of Pape (1974) and of Bradaczek & Luger (1978) are identical within the experimental resolution. In our opinion this indicates the correctness and reliability of the electron-density distributions (Figs. 8–13) because it is very improbable that two such different methods yield the same results in all cases if several solutions were possible. If both methods are applied to the convolution squares of arbitrary centrosymmetric model structures they yield results which are completely identical with each other and with the original electron-density distribution (von Frieling, 1989). Furthermore, the calculated structures were compatible with the expectations. There were nearly constant electron densities in the regions of the aliphatic chains (reasons for the deviation in Fig. 12 are given below), pronounced maxima for the anthracene residues, minima in the middle of the bilayers and sharp electron-density peaks in the cation regions. Using different easier cations, e.g. Ca^{2+}, these peaks were much lower (not shown). The maxima at the origin indicate that there are no or only small water–cation layers between the head groups which cannot be seen at the respective resolution. With barium stearate there is no water included in the head-group region (Lesslauer & Blasie, 1972; Lesslauer, 1974a).

The LB film of 2A7 prepared at a higher surface pressure had a smaller periodicity (Figs. 2, 3, 8 and 9) probably because the molecules tilt against the plane normal in an effort to fill space more effectively. The periodicity of the preparation formed at a lower surface pressure (37·8 Å) is greater than twice the length of a molecule (~36·2 Å) suggesting that the molecules are in a linear conformation and oriented perpendicular to the bilayer plane. The difference can be explained by the gap in the middle and perhaps by a small water–cation layer in the head-group region. A tilted orientation of the molecules or of certain subunits in the former (ten-)bilayer stack ($d = 36$ Å, Fig. 9) is strongly supported by UV–visible spectroscopic measurements indicating an approxi-

mate 30° tilt angle for the anthracene residue (Durfee, Storck, Willig & von Frieling, 1987). Indeed, the projection of the anthracene residue in Fig. 9 is smaller than in Fig. 8. The difference would be compatible with an approximate 30° tilt angle but it must be kept in mind that the resolutions of the two electron-density curves are different.

Both diffraction patterns of the 9,10A12 bilayers (Figs. 4 and 5) show a lower state of order which manifests itself in broader and fewer peaks although the number of the bilayers is the same as for 2A7. This is because the structure of these molecules is disadvantageous for close packing. The 9,10A12 films have similar electron densities in the head-group region (Figs. 10 and 11). Therefore, the differences in the corresponding diffraction patterns must be caused by the different structures in the hydrophobic regions. The measured periodicities (34 or 34·2 Å) are much smaller than twice the length of a molecule (~45·2 Å) but consistent with the measurements of Vincett & Barlow (1980). These researchers discuss in great detail whether the aliphatic chains interpenetrate or randomly coil up. This question is easily answered by Figs. 10 and 11. Both happens but to a different extent depending on the pH value. In Fig. 10 there is an additional maximum on each side of the central minimum apart from those due to the head groups and the anthracene residues. It is probably caused by 'coiled', disordered aliphatic chains. Nevertheless, a part of the fatty acid chains interpenetrates as can be recognized by the broad minimum in the middle with constant electron density. If there were no interpenetration of the fatty-acid chains the central minimum would be much narrower and deeper. The disordered arrangement of the $-CH_2-$ chains is perhaps necessary to fill the space 'under' the bulky anthracene residues.

At pH 6·0 (Fig. 11) obviously the interpenetration increases at the expense of the disordered conformation. The corresponding maxima are much smaller and the central minimum has been lifted. This change of structure is presumably induced by a stronger coordination of the divalent cations (Cd^{2+}) to the carboxyl groups at the higher pH. The general state of order is higher at pH 6. The width at half-height of the fifth-order reflection decreases from $6·0 \times 10^{-3}$ rad at pH 4·9 to $5·3 \times 10^{-3}$ rad at pH 6. Divalent cations generally increase the state of order in LB films (Blodgett, 1935; Blodgett & Langmuir, 1937).

In the electron-density curves of the barium stearate bilayers (Figs. 12 and 13) even the barium layers, the carboxyl and the $-CH_2-$ groups can be seen separately (the resolution is 1·11 Å in Fig. 13). The small wigglings may be partly caused by Fourier series cut-off effects, too, but we consider these effects to be small because we measured a large number of reflections and the intensity of the highest-order reflections approaches zero. In Fig. 13 the hydrophobic region

has the expected constant electron density while the electron density in Fig. 12 slightly increases approaching the centre of the bilayer. In the former case the stearic acid was dissolved in $CHCl_3$, in the latter in petroleum ether. Probably petroleum ether is included in the hydrophobic region of the bilayer in contrast to $CHCl_3$ which obviously evaporates completely. The inclusion of petroleum ether has been presumed before (Lesslauer & Blasie, 1972). The phases of the X-ray reflections of barium stearate bilayers determined in that work are the same as those found by us (alternating +, −, +, −, . . .), the electron-density distribution is compatible with ours at lower resolution.

References

AKERS, C. K. & PARSONS, D. F. (1970). *Biophys. J.* **10**, 116–136.
AUWERAER, M. VAN DER & WILLIG, F. (1985). *Isr. J. Chem.* **25**, 274–278.
BLAUROCK, A. E. & WORTHINGTON, C. R. (1966). *Biophys. J.* **6**, 305–312.
BLODGETT, K. B. (1935). *J. Am. Chem. Soc.* **57**, 1007–1022.
BLODGETT, K. B. & LANGMUIR, I. (1937). *Phys. Rev.* **51**, 964–982.
BRADACZEK, H. & LUGER, P. (1978). *Acta Cryst.* **A34**, 681–683.
DURFEE, W. S., STORCK, W., WILLIG, F. & VON FRIELING, M. (1987). *J. Am. Chem. Soc.* **109**, 1297–1301.
EWALD, P. P. (1940). *Proc. Phys. Soc. London*, **52**, 167–174.
FRANKS, N. P., ARUNACHALAM, T. & CASPI, E. (1978). *Nature (London)*, **276**, 530–532.
FRANKS, N. P. & LEVINE, Y. K. (1981). *Membrane Spectroscopy*, edited by E. GRELL, pp. 437–489. Berlin: Springer-Verlag.
FRANKS, N. P. & LIEB, W. R. (1979). *J. Mol. Biol.* **133**, 469–500.
FRIELING, M. VON (1989). *Strukturuntersuchungen an synthetischen Lipiden und bakteriellen Endotoxinen.* Doctoral Dissertation, Freie Universität, Berlin, Federal Republic of Germany.
FROMHERZ, P. (1975). *Rev. Sci. Instrum.* **46**(10), 1380–1385.
HOSEMANN, R. & BAGCHI, S. N. (1952). *Acta Cryst.* **5**, 749–762.
HOSEMANN, R. & BAGCHI, S. N. (1953). *Acta Cryst.* **6**, 318–325.
HOSEMANN, R. & BAGCHI, S. N. (1962). *Direct Analysis of Diffraction by Matter.* Amsterdam: North Holland.
KREUTZ, W. (1970). *Advances in Botanical Research* 3, edited by R. D. PRESTON, pp. 53–169. New York: Academic Press.
LESSLAUER, W. (1974a). *Acta Cryst.* **B30**, 1927–1931.
LESSLAUER, W. (1974b). *Acta Cryst.* **B30**, 1932–1937.
LESSLAUER, W. & BLASIE, J. K. (1972). *Biophys. J.* **12**, 175–190.
LESSLAUER, W., CAIN, J. & BLASIE, J. K. (1971). *Biochim. Biophys. Acta*, **241**, 547–566.
LUZATTI, V., TARDIEU, A. & TAUPIN, D. (1972). *J. Mol. Biol.* **64**, 269–286.
PAPE, E. H. (1974). *Biophys. J.* **14**, 284–294.
TARDIEU, A., LUZATTI, V. & REMAN, F. C. (1973). *J. Mol. Biol.* **75**, 711–733.
VINCETT, P. S. & BARLOW, W. A. (1980). *Thin Solid Films*, **71**, 305–326.
WORTHINGTON, C. R. (1969). *Biophys. J.* **9**, 222–234.
WORTHINGTON, C. R. (1973a). *Current Topics in Bioenergetics*, edited by B. R. SANADI & L. PACHER, Vol. V, pp. 1–39. New York: Academic Press.
WORTHINGTON, C. R. (1973b). *Exp. Eye Res.* **17**, 487–501.
WORTHINGTON, C. R., KING, G. J. & McINTOSH, T. J. (1973). *Biophys. J.* **13**, 480–494.